

Dark energy driven by an oscillating generalised axion-like quintessence field

Mariam Bouhmadi-López^{1,2,3, a} and Carlos G. Boiza^{2,3, b}

¹*IKERBASQUE, Basque Foundation for Science, 48011, Bilbao, Spain*

²*Department of Physics, University of the Basque Country UPV/EHU, P.O. Box 644, 48080 Bilbao, Spain*

³*EHU Quantum Center, University of the Basque Country UPV/EHU, P.O. Box 644, 48080 Bilbao, Spain*

Generalised axion-like scalar fields provide a well-motivated framework for describing the late-time acceleration of the Universe. As the field evolves, it rolls down its potential and, depending on its mass and initial conditions, it may either still be approaching the minimum or already oscillating around it. These two dynamical regimes require distinct treatments of cosmological perturbations. In this work, we perform a detailed analysis of linear cosmological perturbations in the regime where the dark-energy scalar field undergoes coherent oscillations about the minimum of its potential. We show that the standard effective fluid description breaks down in this phase and develop a consistent field-based perturbation framework, which we use to assess the impact of oscillatory dark energy on the growth of cosmic structures.

I. INTRODUCTION

Quintessence provides a theoretically well-motivated framework for explaining the late-time accelerated expansion of the Universe by postulating a canonical scalar field minimally coupled to gravity [1, 2]. Unlike a cosmological constant, whose energy density is strictly time independent, quintessence is intrinsically dynamical: its evolution is governed by a self-interaction potential, allowing the equation-of-state parameter to vary with cosmic time, typically remaining close to, but not exactly equal to, $w = -1$ [3]. As a result, quintessence models offer a dynamical origin for dark energy and can, at least partially, alleviate conceptual issues of the Λ CDM paradigm such as fine-tuning and cosmic coincidence, while remaining consistent with current observational constraints [1, 2, 4–8]. Beyond their impact on the background expansion history, such models can also leave observable signatures in the growth of cosmic structures [9, 10].

For a canonical, minimally coupled scalar field, several well-defined dynamical routes exist through which an effective equation of state approaching $w \rightarrow -1$ can be realised. A broad and well-studied class of such models is given by freezing scenarios, in which the scalar field initially has $w > -1$ and evolves toward $w \simeq -1$ with $dw/dt < 0$ as the kinetic contribution progressively decreases. Within this class, tracking and scaling solutions allow the scalar field to follow the background evolution during radiation and matter domination before transitioning to a dark-energy-dominated phase, thereby helping to alleviate the coincidence problem [5–7]. In most well-studied freezing models of this type, the de Sitter-like attractor is realised only in a runaway regime at $\phi \rightarrow \infty$, and the potential does not admit a finite, positive minimum.

By contrast, in thawing models the scalar field remains

frozen by Hubble friction until relatively late-time, maintaining $w \simeq -1$ over most of the observationally relevant epoch [11–13]. Once the field begins to roll, the equation of state departs from -1 with $dw/dt > 0$, reflecting the growth of the kinetic energy. In all these cases, the emergence of $w \simeq -1$ is a natural dynamical outcome of scalar-field evolution rather than the result of a finely tuned cosmological constant [8].

Observationally, current data tightly constrain departures from $w = -1$ at late-time, but do not uniquely determine the nature of dark energy. Taken individually, key probes—Type Ia supernovae, baryon acoustic oscillations, the cosmic microwave background, and large-scale structure—are broadly consistent with an equation of state close to $w = -1$, and typically allow only limited room for mild evolution within their standalone uncertainties [14–22]. Joint analyses provide substantially tighter constraints and can, depending on the adopted data combination and systematics, either further restrict late-time evolution or mildly prefer it within time-dependent parameterisations. In previous works [23, 24], we showed that scalar fields with generalised axion-like potentials achieve statistical parity with Λ CDM according to Bayesian model comparison and information criteria (see also [25]). Moreover, recent results from the Dark Energy Spectroscopic Instrument (DESI), including its second data release, have further strengthened interest in dynamical dark energy: combined analyses of DESI baryon acoustic oscillation data with external probes indicate that evolving dark-energy models can fit the data at a level comparable to Λ CDM, with the strength of any preference depending on the particular combination employed [26–29]. These developments motivate a careful and robust treatment of scalar-field dynamics and their imprint on structure formation.

Axion dark energy represents a theoretically appealing realisation of dynamical dark energy, in which a light pseudoscalar field drives late-time cosmic acceleration through its potential [30–33]. Within this broader class, generalised axion-like models provide a flexible phenomenological framework capable of producing a rich variety of late-time behaviours while remaining compat-

^a mariam.bouhmadi@ehu.eus

^b carlos.garciab@ehu.eus

ible with current observations [23–25, 34–36]. Beyond their role as dark-energy candidates, axion and axion-like scalar fields have been widely explored in cosmology and particle physics, with applications ranging from early-dark-energy scenarios connected to the Hubble tension [37, 38] and modifications of the recombination-era dynamics [39], to inflationary model building [40], primordial black-hole formation mechanisms [41], and dark-matter phenomenology in both QCD-inspired and ultra-light regimes [42, 43]. Axion-motivated multi-field realisations, such as the string axiverse, further illustrate how a spectrum of light fields can give rise to rich cosmological dynamics across cosmic history [31, 32], and dedicated numerical simulations have been developed to characterise the distinctive clustering properties of ultra-light axion dark matter [44–46].

In many well-studied tracking quintessence models, such as inverse power-law potentials, the scalar field evolves along a runaway direction in field space and approaches a de Sitter-like state only in the limit $\phi \rightarrow \infty$, without the presence of a finite positive minimum of the potential [1, 5–7]. By contrast, a distinctive feature of the class of models considered in this work is that the de Sitter state is realised at a finite field value, corresponding to a true positive minimum of the potential [35, 36]. As the scalar field relaxes toward this minimum, it may overshoot and oscillate coherently around it. This behaviour differs qualitatively from the monotonic approach to de Sitter characteristic of runaway tracking models and has important consequences for cosmological perturbations: at the turning points of the oscillatory motion, the effective fluid description of dark energy becomes ill defined, even though the underlying scalar-field and metric perturbations remain perfectly regular.

In this work we focus on the oscillatory regime of generalised axion-like quintessence and develop a consistent linear perturbation framework that remains well defined across both oscillatory and non-oscillatory phases. By working directly with the fundamental scalar-field and metric perturbations, we avoid the pathologies of the effective fluid approach and obtain a robust description of the impact of oscillatory dark energy on the growth of cosmic structures.

This paper is organised as follows. In Section II, we introduce the generalised axion-like quintessence model and summarise its background dynamics. In Section III, we derive the linear cosmological perturbation equations appropriate for oscillatory scalar-field dynamics. In Section IV, we present and analyse numerical solutions of the perturbation equations and discuss their implications for the growth of cosmic structures. Finally, in Section V, we summarise our main results and draw our conclusions.

II. GENERALISED AXION-LIKE QUINTESSENCE WITH MATTER AND RADIATION

In this section we summarise the quintessence model introduced in [34, 35], which generalises axion-like scalar-field potentials to describe the late-time accelerated expansion of the Universe. The model is formulated within a spatially flat Friedmann–Lemaître–Robertson–Walker (FLRW) cosmology and includes standard radiation and pressureless matter components, which dominate the cosmic expansion at early-time and provide the background against which the scalar-field dynamics unfold.

A. Background dynamics

We consider a canonical scalar field ϕ minimally coupled to gravity, evolving in a spatially flat FLRW spacetime with line element

$$ds^2 = -dt^2 + a^2(t) \delta_{ij} dx^i dx^j, \quad (1)$$

where $a(t)$ is the cosmological scale factor, and coexisting with standard radiation and pressureless matter.

The action of the system is

$$S = \int d^4x \sqrt{-g} \left[\frac{1}{2\kappa^2} R - \frac{1}{2} g^{\mu\nu} \partial_\mu \phi \partial_\nu \phi - V(\phi) \right] + S_r + S_m, \quad (2)$$

where $\kappa^2 \equiv 8\pi G$, and S_r and S_m denote the actions for the radiation and matter components, respectively.

Variation of the action with respect to the scalar field yields the homogeneous Klein–Gordon equation,

$$\ddot{\phi} + 3H\dot{\phi} + V_{,\phi} = 0, \quad (3)$$

where $V_{,\phi} \equiv dV/d\phi$, and the Hubble parameter $H \equiv \dot{a}/a$ is defined in terms of the scale factor.

The expansion of the Universe is governed by the Friedmann equations,

$$H^2 = \frac{\kappa^2}{3} (\rho_r + \rho_m + \rho_\phi), \quad (4)$$

$$\dot{H} = -\frac{\kappa^2}{2} \left(\frac{4}{3} \rho_r + \rho_m + \rho_\phi + p_\phi \right), \quad (5)$$

where the scalar field behaves as an effective perfect fluid with energy density and pressure

$$\rho_\phi = \frac{1}{2} \dot{\phi}^2 + V(\phi), \quad p_\phi = \frac{1}{2} \dot{\phi}^2 - V(\phi). \quad (6)$$

Radiation and pressureless matter satisfy the standard continuity equations,

$$\dot{\rho}_r + 4H\rho_r = 0, \quad \dot{\rho}_m + 3H\rho_m = 0, \quad (7)$$

so that radiation dominates the expansion at early-time, followed by a matter-dominated era, while the scalar field becomes dynamically relevant only at late-time.

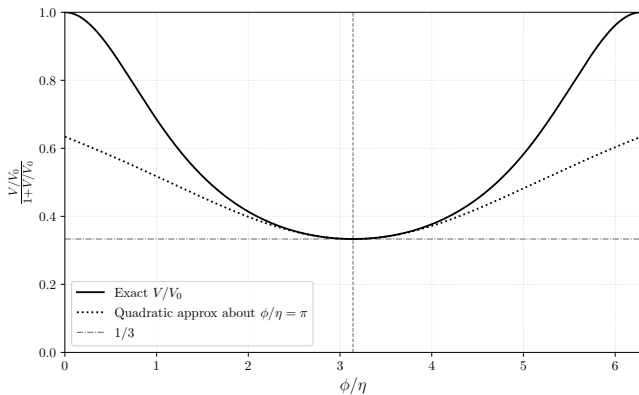


Figure 1: Exact generalised axion-like potential $V(\phi)/V_0 = [1 - \cos(\phi/\eta)]^{-n}$ (solid line) and its quadratic approximation around the minimum at $\phi/\eta = \pi$ (dotted line), shown as functions of the dimensionless field variable ϕ/η for the representative case $n = 1$. The potential is displayed in the compactified form $(V/V_0)/(1 + V/V_0)$ in order to avoid divergences at the extrema. In this representation, the minimum of the potential corresponds to $(V/V_0)/(1 + V/V_0) = 1/3$.

This framework provides the minimal and well-established setting for quintessence models of dark energy, within which the specific properties of the scalar-field potential determine the detailed late-time cosmological dynamics.

B. Generalised axion-like potential and effective mass

The dynamics of the scalar field are governed by a generalised axion-like potential of the form

$$V(\phi) = V_0 \left[1 - \cos\left(\frac{\phi}{\eta}\right) \right]^{-n}, \quad V_0 > 0, \quad n > 0, \quad \eta > 0. \quad (8)$$

Here V_0 sets the overall energy scale of the potential and η is a constant with dimensions of mass. The conditions $V_0 > 0$, $n > 0$, and $\eta > 0$ ensure that the potential is positive definite and admits a well-defined minimum. This potential generalises the standard axion-like form commonly considered in quintessence and dark-energy models [30–33], and is treated here as an effective phenomenological description of the scalar-field self-interactions.

For suitable parameter choices, the potential admits a prolonged dynamical regime in which the scalar field tracks the dominant background component during radiation- and matter-dominated eras, before eventually driving late-time cosmic acceleration, as discussed in [35]. The overall shape of the potential and its behaviour near the minimum are illustrated in Fig. 1 for the representative case $n = 1$.

The potential (8) possesses a minimum at

$$\phi_{\min} = \pi\eta, \quad (9)$$

where the first derivative of the potential vanishes. The value of the potential at the minimum is given by

$$V_{\min} \equiv V(\phi_{\min}) = 2^{-n} V_0. \quad (10)$$

For the illustrative case $n = 1$ shown in Fig. 1, this corresponds to $V_{\min}/V_0 = 1/2$.

Expanding the potential around the minimum yields

$$V(\phi) \simeq V_{\min} + \frac{1}{2} m_{\text{eff}}^2 (\phi - \phi_{\min})^2 + \mathcal{O}[(\phi - \phi_{\min})^3], \quad (11)$$

which defines the effective mass of the scalar field,

$$m_{\text{eff}}^2 \equiv V_{,\phi\phi}|_{\phi=\phi_{\min}} = \frac{n}{2\eta^2} V_{\min}. \quad (12)$$

Such a quadratic expansion around the minimum and the associated effective mass are standard in the analysis of coherently oscillating scalar fields in cosmology [33]. Equation (12) shows explicitly that the effective mass is determined by the curvature of the potential at its minimum and by the vacuum energy scale V_{\min} . In particular, increasing n or decreasing η leads to a larger m_{eff} , thereby favouring an earlier onset of oscillatory behaviour once the field reaches the vicinity of the minimum. Near ϕ_{\min} , the quadratic approximation provides an accurate description of the local dynamics of the scalar field and captures the essential features of the oscillatory regime.

C. Tracking behaviour, late-time acceleration, and oscillatory criterion

The cosmological evolution of the generalised axion-like scalar field typically proceeds through an early-time tracking regime followed by a late-time phase in which the field becomes dominant and drives cosmic acceleration. Importantly, the early-time tracking behaviour of this model is *not* a scaling solution: although the scalar-field energy density remains subdominant and evolves in a manner largely insensitive to initial conditions, the scalar-field equation of state does not, in general, coincide with that of the dominant background component.

During matter domination, the tracker solution is well approximated by [35, 36]

$$w_\phi \simeq -\frac{1}{1+n}, \quad (\text{matter domination}), \quad (13)$$

so that the scalar-field equation of state depends explicitly on the potential parameter n . In particular, for $n = 1$ one obtains $w_\phi \simeq -1/2$, while smaller values of n yield w_ϕ closer to -1 , making the background evolution increasingly similar to that of a cosmological constant already during the tracking phase. In this regime, the scalar-field energy density decreases more slowly than

that of matter, allowing Ω_ϕ to grow with time and naturally triggering a transition to dark-energy domination at late-time.

As the field approaches the minimum of the potential, the dynamics become controlled by the local curvature scale, characterised by the effective mass m_{eff} defined in Eq. (12). Once the field is sufficiently close to the minimum $\phi_{\text{min}} = \pi\eta$, the field displacement $\Delta_\phi \equiv \phi - \phi_{\text{min}}$ satisfies, to leading order,

$$\ddot{\Delta}_\phi + 3H\dot{\Delta}_\phi + m_{\text{eff}}^2 \Delta_\phi \simeq 0, \quad (14)$$

which corresponds to a damped harmonic oscillator with Hubble friction. If H is approximately constant over an oscillation period, the ansatz $\Delta_\phi \propto e^{\lambda t}$ gives

$$\lambda_\pm = -\frac{3H}{2} \pm \sqrt{\left(\frac{3H}{2}\right)^2 - m_{\text{eff}}^2}. \quad (15)$$

The motion is underdamped (and therefore oscillatory) only when the discriminant is negative, i.e.

$$m_{\text{eff}} > \frac{3}{2}H. \quad (16)$$

Since $H(t)$ varies slowly at late-time and the transition from overdamped to underdamped behaviour is gradual, it is useful to express this as an order-of-magnitude diagnostic in terms of the present-day expansion rate H_0 . This motivates

$$\begin{aligned} m_{\text{eff}} \gtrsim H_0 &\Rightarrow \text{oscillations are possible by today,} \\ m_{\text{eff}} \lesssim H_0 &\Rightarrow \text{the field remains overdamped,} \end{aligned} \quad (17)$$

where the second line follows because in the overdamped regime the solution is a sum of two decaying exponentials rather than a sinusoid.

A useful corollary of Eq. (17) is that it implies an order-of-magnitude critical scale η_{crit} separating models that have already entered coherent oscillations by the time the field reaches the vicinity of the minimum from those that remain overdamped. Using Eq. (12), the oscillation condition $m_{\text{eff}} \sim \mathcal{O}(H)$ can be written as $\eta \sim \sqrt{nV_{\text{min}}}/H$. If, in addition, the field reaches the minimum during the onset of vacuum-energy domination so that $3H^2 \simeq \kappa^2 V_{\text{min}}$, the dependence on V_{min} cancels and one finds $\eta_{\text{crit}} \sim \sqrt{n}\kappa^{-1}$. In this approximation, η_{crit} is therefore set primarily by the gravitational scale κ^{-1} (up to an $\mathcal{O}(1)$ factor depending on n) and is only weakly sensitive to late-time cosmological parameters such as H_0 and Ω_{m0} . More generally, if the minimum is reached when matter, radiation, or the scalar kinetic term still contribute non-negligibly to the expansion rate, $3H^2 \simeq \kappa^2 (V_{\text{min}} + K + \rho_m + \rho_r)$, the cancellation is only approximate and η_{crit} acquires mild corrections of relative size $\sim [1 + K/V_{\text{min}} + (\rho_m + \rho_r)/V_{\text{min}}]^{-1/2}$. In the late-time accelerating regime relevant for the oscillatory solutions studied here, one typically has $w_\phi \simeq -1$, so that $K \ll V_{\text{min}}$ and matter is already subdominant, keeping

the dependence of η_{crit} on these details modest in practice.

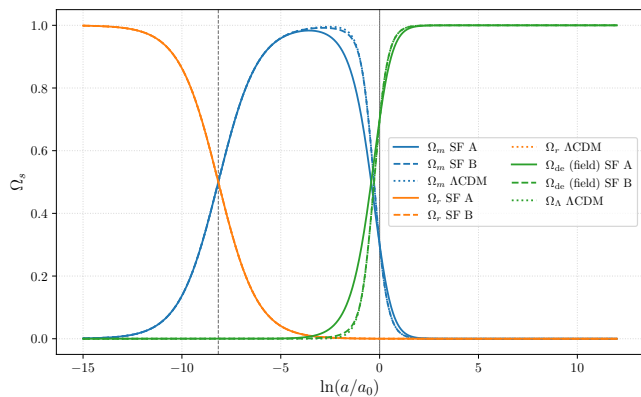
The background evolution for representative models is illustrated in Fig. 2. The left panel shows the evolution of the density parameters, including the growth of Ω_ϕ during the tracking phase and the transition to scalar-field domination at late-time. The right panel displays the corresponding evolution of the scalar-field equation-of-state parameter, highlighting both the non-scaling nature of the tracking regime and the late-time approach towards $w_\phi \simeq -1$ as the field settles near the potential minimum.¹

It is worth emphasising that the presence of a late-time oscillatory regime constitutes a distinctive feature of the generalised axion-like potential considered here. In many well-studied tracking quintessence models, such as inverse power-law potentials, late-time cosmic acceleration arises from an asymptotic evolution in which the scalar field rolls monotonically towards $\phi \rightarrow \infty$, with no minimum and therefore no oscillatory behaviour [5–7]. In those cases, the tracking solution smoothly connects to a slow-roll-like dark-energy phase, and the fluid description of perturbations remains well defined at all times.

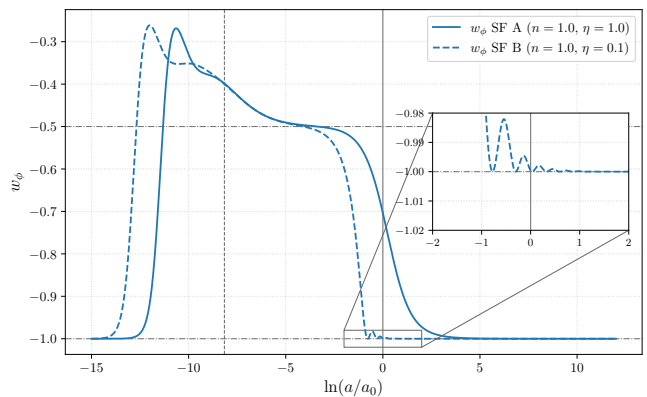
By contrast, the generalised axion-like potential admits a finite minimum that can be reached at late-time, opening the possibility of coherent oscillations precisely during the dark-energy-dominated epoch. This feature places the model outside the standard quintessence paradigm and necessitates a careful reassessment of both background and perturbative dynamics in the late Universe.

The distinction between oscillatory and non-oscillatory regimes has important implications for the treatment of cosmological perturbations. In the absence of oscillations ($m_{\text{eff}} \lesssim H_0$), the scalar field evolves slowly and can be consistently described as an effective dark-energy fluid, allowing the use of a multi-fluid perturbation framework in which both the equation-of-state parameter w_ϕ and the adiabatic sound speed remain finite and slowly varying. In this case, the modified clustering properties of dark energy generically lead to a suppression of matter per-

¹ All numerical results and figures in this section are computed for $n = 1$. The background evolution is obtained by integrating the homogeneous equations with initial conditions $\phi_i/\eta = 10^{-4}$ and $\dot{\phi}_i = 0$. Owing to the presence of an early-time tracking regime, the late-time evolution of the scalar field is largely insensitive to the precise choice of these initial conditions; the values adopted here are therefore chosen for numerical stability and convenience. We fix the present-day matter density parameter to $\Omega_{m0} = 0.3$. The present-day Hubble parameter is fixed to $H_0 = 69.5705 \text{ km s}^{-1} \text{ Mpc}^{-1}$, corresponding to $h \equiv H_0/(100 \text{ km s}^{-1} \text{ Mpc}^{-1})$, a value that lies between the cosmic-microwave-background-inferred determination from [17] and recent Type Ia supernova measurements [16]. The radiation density is set using $\Omega_{r0} = \Omega_{m0}/(1 + z_{\text{eq}})$, with $z_{\text{eq}} = 2.5 \times 10^4 (\Omega_{m0} h^2) (T_{\text{CMB}}/2.7)^{-4}$ and $T_{\text{CMB}} = 2.7255 \text{ K}$ [47, 48]. The parameter V_0 is chosen such that the closure relation $\Omega_{m0} + \Omega_{r0} + \Omega_{\phi0} = 1$ is satisfied.



(a) Evolution of the density parameters Ω_m , Ω_r , and Ω_ϕ for two representative generalised axion-like quintessence models, corresponding to $\eta = 1$ (non-oscillatory) and $\eta = 0.1$ (oscillatory). During the tracking phase the scalar-field density fraction grows relative to matter, eventually dominating the cosmic expansion and driving late-time acceleration.



(b) Evolution of the density parameters Ω_m , Ω_r , and Ω_ϕ for the two benchmark models shown throughout this work: SF A ($\eta = 1$, non-oscillatory) and SF B ($\eta = 0.1$, oscillatory). During the tracking phase the scalar-field density fraction grows relative to matter, eventually dominating the cosmic expansion and driving late-time acceleration.

Figure 2: Background evolution of generalised axion-like quintessence. The left panel shows the transition from radiation and matter domination to a scalar-field-dominated accelerated phase, while the right panel shows the associated evolution of the scalar-field equation of state. The comparison highlights the qualitative difference between the non-oscillatory benchmark SF A ($\eta = 1$) and the oscillatory benchmark SF B ($\eta = 0.1$) at late-time.

turbations, with potentially observable consequences for the growth of structure and related cosmological probes.

Once coherent oscillations are present ($m_{\text{eff}} \gtrsim H_0$), this description breaks down. Although the instantaneous equation of state $w_\phi = p_\phi/\rho_\phi$ remains well defined throughout the evolution, the adiabatic sound speed $c_{a\phi}^2 \equiv \dot{p}_\phi/\dot{\rho}_\phi$ diverges whenever $w_\phi = -1$, which necessarily occurs at each turning point of the oscillatory motion around the potential minimum. As a result, the adiabatic sound speed entering the fluid perturbation equations becomes ill defined, rendering the standard multi-fluid description inconsistent in the oscillatory regime [36]. At the background level, however, the oscillatory solutions are characterised by an equation of state that remains very close to $w_\phi \simeq -1$ once the scalar field becomes dynamically relevant. Consequently, the scalar field behaves effectively as a cosmological constant from the perspective of structure formation, strongly suppressing the impact of dark-energy perturbations on the growth of matter fluctuations.

These two behaviours are explicitly illustrated by the benchmark models shown in Figs. 2a and 2b. For SF A ($\eta = 1$, measured in units of the gravitational scale κ^{-1}), the effective mass satisfies $m_{\text{eff}} \lesssim H_0$, and the field has not completed a full oscillation by the present epoch. In this case the scalar field remains in a non-oscillatory regime with w_ϕ appreciably different from -1 for an extended period, during which it contributes non-negligibly to the total energy density and modifies the expansion history, leading to a potentially observable suppression of matter clustering. By contrast, for SF B ($\eta = 0.1$) one finds $m_{\text{eff}} \gtrsim H_0$, so that coherent oscillations are al-

ready present today. The scalar field then settles into an evolution with $w_\phi \simeq -1$ on average, and both the background dynamics and the associated matter perturbations closely mimic those of Λ CDM, making deviations in late-time clustering significantly less apparent.

Nevertheless, oscillatory solutions cannot be disregarded on phenomenological grounds. Indeed, our analysis of observational data in [23] revealed a bimodal structure in the allowed parameter space, encompassing both non-oscillatory models—such as the $\eta = 1$ case—and oscillatory models, exemplified by $\eta = 0.1$.

These considerations motivate a unified perturbative treatment that remains valid across both regimes and does not rely on a fluid approximation. In the following section we therefore develop the linear perturbation equations directly at the level of the scalar field and metric fluctuations, enabling a consistent and robust assessment of generalised axion-like quintessence models across the full parameter space.

III. COSMOLOGICAL PERTURBATIONS WITH OSCILLATING SCALAR FIELDS

In this section we develop the linear cosmological perturbation theory for generalised axion-like quintessence models in the presence of coherent scalar-field oscillations. As discussed in Sec. II C, the late-time dynamics of these models can enter an oscillatory regime in which the usual effective fluid description of dark energy breaks down. In particular, although the background evolution remains well behaved, the adiabatic sound speed asso-

ciated with a fluid approximation becomes ill defined whenever the scalar-field equation of state approaches $w_\phi = -1$, which inevitably occurs during each oscillation around the minimum of the potential.

To overcome this limitation, we formulate the perturbation equations directly in terms of the fundamental scalar-field and metric fluctuations, without relying on a multi-fluid description of dark energy. This approach remains well defined in both oscillatory and non-oscillatory regimes and allows for a consistent treatment of perturbations across the entire parameter space of the model.

In this section we focus on the theoretical formulation of the perturbation equations and on their general properties. A detailed numerical analysis of scalar-field and matter perturbations, as well as their impact on observable quantities such as the matter power spectrum and the growth-rate parameter $f\sigma_8$, is presented in the following section. Further technical aspects of the breakdown of the fluid description in the oscillatory regime, together with additional numerical diagnostics, are discussed in Appendix A.

Cosmological perturbations have been extensively studied in the literature in a variety of contexts; see, for instance, [49–56] for general reviews and formulations. In particular, [57] presents a closely related treatment of perturbations, employing a notation and gauge choice similar to the one adopted in this work.

A. Linear perturbations and gauge choice

We study scalar perturbations around a spatially flat FLRW background in the Newtonian gauge. The perturbed line element is

$$ds^2 = a^2(\tau) \left[-(1 + 2\Phi) d\tau^2 + (1 - 2\Psi) \delta_{ij} dx^i dx^j \right], \quad (18)$$

where τ denotes conformal time, related to cosmic time by $d\tau = dt/a$, and $\Phi(\tau, \mathbf{x})$ and $\Psi(\tau, \mathbf{x})$ are the Bardeen potentials [58]. Throughout this work we assume negligible anisotropic stress for the matter and radiation components, so that

$$\Phi = \Psi. \quad (19)$$

We work in Fourier space, where each perturbation variable $X(\tau, \mathbf{x})$ is decomposed as $X(\tau, \mathbf{x}) = \int d^3k X(\tau, \mathbf{k}) e^{i\mathbf{k}\cdot\mathbf{x}}$ and the Laplacian acts as $\nabla^2 \rightarrow -k^2$.

The scalar field is perturbed as

$$\phi(\tau, \mathbf{x}) = \bar{\phi}(\tau) + \delta\phi(\tau, \mathbf{x}), \quad (20)$$

where an overbar denotes the homogeneous background. The background field obeys the Klein–Gordon equation

$$\bar{\phi}'' + 2\mathcal{H}\bar{\phi}' + a^2 V_{,\phi}(\bar{\phi}) = 0, \quad (21)$$

with $\mathcal{H} \equiv a'/a$ the conformal Hubble rate and a prime denoting $d/d\tau$.

Einstein equations at linear order

The linearised Einstein equations in the Newtonian gauge yield the usual constraint and evolution equations for Ψ [56]. The $(0, 0)$ component gives

$$k^2 \Psi + 3\mathcal{H}(\Psi' + \mathcal{H}\Psi) = -4\pi G a^2 \delta\rho, \quad (22)$$

while the $(0, i)$ component implies

$$\Psi' + \mathcal{H}\Psi = -4\pi G a^2 (\bar{\rho} + \bar{p}) v, \quad (23)$$

where $\delta\rho$ is the total energy-density perturbation and v is the total velocity potential defined through $\delta T^0_i = (\bar{\rho} + \bar{p}) \partial_i v$. Finally, the traceless (i, j) equation enforces Eq. (19) in the absence of anisotropic stress, and the trace part provides the dynamical equation

$$\Psi'' + 3\mathcal{H}\Psi' + (2\mathcal{H}' + \mathcal{H}^2) \Psi = 4\pi G a^2 \delta p, \quad (24)$$

with δp the total pressure perturbation.

The total perturbed sources are the sums over matter, radiation, and the scalar field:

$$\delta\rho = \delta\rho_m + \delta\rho_r + \delta\rho_\phi, \quad (25)$$

$$\delta p = \delta p_r + \delta p_\phi, \quad (26)$$

$$(\bar{\rho} + \bar{p}) v = \sum_A (\bar{\rho}_A + \bar{p}_A) v_A. \quad (27)$$

where $A \in \{m, r, \phi\}$ and $\bar{p}_m = 0$, $\bar{p}_r = \bar{\rho}_r/3$.

Scalar-field perturbation equation

The perturbation $\delta\phi$ is governed by the linearised Klein–Gordon equation in the Newtonian gauge [53–55],

$$\delta\phi'' + 2\mathcal{H}\delta\phi' + (k^2 + a^2 V_{,\phi\phi}(\bar{\phi})) \delta\phi = 4\bar{\phi}'\Psi' - 2a^2 V_{,\phi}(\bar{\phi}) \Psi, \quad (28)$$

which remains well defined even when $\bar{\phi}'$ crosses zero during coherent oscillations.

For completeness, it is useful to recall the scalar-field contributions to the perturbed energy-momentum tensor in this gauge:

$$\delta\rho_\phi = \frac{1}{a^2} (\bar{\phi}' \delta\phi' - \bar{\phi}'^2 \Psi) + V_{,\phi}(\bar{\phi}) \delta\phi, \quad (29)$$

$$\delta p_\phi = \frac{1}{a^2} (\bar{\phi}' \delta\phi' - \bar{\phi}'^2 \Psi) - V_{,\phi}(\bar{\phi}) \delta\phi, \quad (30)$$

$$(\bar{\rho}_\phi + \bar{p}_\phi) v_\phi = -\frac{\bar{\phi}'}{a^2} \delta\phi, \quad (31)$$

where the last relation follows from $\delta T^0_{i(\phi)} = -\bar{\phi}' \partial_i \delta\phi/a^2$. These expressions allow us to close the Einstein system Eqs. (22)–(24) in terms of the dynamical variables $(\Psi, \delta\phi)$ and the matter/radiation perturbations.

Matter and radiation perturbations

We model radiation and pressureless matter as perfect fluids obeying $\nabla_\mu T^\mu{}_\nu(A) = 0$ at linear order. In the Newtonian gauge, their continuity and Euler equations in Fourier space can be written as [57]

$$\delta'_r - \frac{4}{3}(k^2 v_r + 3\Psi') = 0, \quad v'_r + \frac{1}{4}\delta_r + \Psi = 0, \quad (32)$$

$$\delta'_m - (k^2 v_m + 3\Psi') = 0, \quad v'_m + \mathcal{H}v_m + \Psi = 0, \quad (33)$$

where $\delta_A \equiv \delta\rho_A/\bar{\rho}_A$ and the velocity potentials are defined via $\delta T^0{}_{i(A)} = (\bar{\rho}_A + \bar{p}_A)\partial_i v_A$.

Equations (22)–(33), together with the background system, provide a closed set of linear perturbation equations once a choice of initial conditions is specified. In the next subsection we explain why, in the oscillatory regime, treating the scalar field as an effective fluid leads to a breakdown of the standard multi-fluid formulation, and we motivate the field-based approach adopted here.

B. Breakdown of the multi-fluid description in the oscillatory regime

In the non-oscillatory regime of quintessence, where the scalar field evolves monotonically and remains slow rolling at late-time, it is often convenient to describe the scalar field as an effective dark-energy fluid. In this picture, the field is characterised by an equation-of-state parameter $w_\phi \equiv p_\phi/\rho_\phi$ together with an adiabatic sound speed $c_{a\phi}^2 \equiv \dot{p}_\phi/\dot{\rho}_\phi$ and an effective (rest-frame) sound speed $c_{s\phi}^2 = 1$. This framework was successfully employed in our previous work [36] to study linear perturbations in the tracking and non-oscillatory regimes.

However, once the scalar field enters a regime of coherent oscillations around the minimum of its potential, the effective fluid description ceases to be valid. This breakdown is not associated with any pathology of the underlying field theory, but rather with the failure of the fluid variables used to describe it.

Divergence of the adiabatic sound speed

The key quantity responsible for the breakdown of the fluid picture is the adiabatic sound speed,

$$c_{a\phi}^2 \equiv \frac{\dot{p}_\phi}{\dot{\rho}_\phi}. \quad (34)$$

For a canonical scalar field,

$$\rho_\phi = \frac{1}{2}\dot{\phi}^2 + V(\phi), \quad p_\phi = \frac{1}{2}\dot{\phi}^2 - V(\phi), \quad (35)$$

so that

$$\dot{\rho}_\phi = \dot{\phi}(\ddot{\phi} + V_{,\phi}), \quad \dot{p}_\phi = \dot{\phi}(\ddot{\phi} - V_{,\phi}). \quad (36)$$

Using the background Klein–Gordon equation $\ddot{\phi} + 3H\dot{\phi} + V_{,\phi} = 0$, one finds

$$c_{a\phi}^2 = 1 + \frac{2V_{,\phi}}{3H\dot{\phi}}. \quad (37)$$

In the oscillatory regime, the scalar field crosses the minimum of the potential repeatedly. At each turning point of the oscillation,

$$\dot{\phi} = 0, \quad w_\phi = -1, \quad (38)$$

while $V_{,\phi}$ remains finite. As a result, the adiabatic sound speed $c_{a\phi}^2$ diverges at each oscillation. Since $c_{a\phi}^2$ enters explicitly into the fluid perturbation equations, this divergence renders the multi-fluid system ill defined.

Importantly, this divergence does *not* signal a physical instability of the underlying theory. Rather, it reflects a breakdown of the effective fluid variables used to describe the scalar field. In particular, while the density perturbation δ_ϕ remains finite throughout the evolution, the velocity potential v_ϕ becomes ill defined whenever $\dot{\phi} = 0$, as it is proportional to $\delta\phi/\dot{\phi}$. These points correspond to the turning points of the oscillatory motion, where the scalar field momentarily behaves as a pure cosmological constant with $w_\phi = -1$. The fundamental field perturbation $\delta\phi$, as well as the metric perturbations, remain perfectly regular across these crossings (see Appendix A); only the mapping from field variables to effective fluid variables fails.

Failure of the effective fluid perturbation equations

In the fluid approach, scalar-field perturbations are usually evolved through equations of the form [36]

$$\delta'_\phi = -3\mathcal{H}(c_{s\phi}^2 - w_\phi)\delta_\phi + (1 + w_\phi)(k^2 v_\phi + 3\Psi') + 9\mathcal{H}^2(c_{s\phi}^2 - c_{a\phi}^2)(1 + w_\phi)v_\phi, \quad (39)$$

$$v'_\phi = -\mathcal{H}(1 - 3c_{s\phi}^2)v_\phi - \frac{c_{s\phi}^2}{1 + w_\phi}\delta_\phi - \Psi, \quad (40)$$

where primes denote derivatives with respect to conformal time. In the oscillatory regime, these equations become ill defined due to:

- divergences in $c_{a\phi}^2$,
- the vanishing of $1 + w_\phi$ at turning points.

As a consequence, numerical integration of the fluid equations becomes unstable and physically unreliable, even though the true perturbations of the scalar field remain finite and well behaved.

Field-based perturbation approach

To consistently describe perturbations in the oscillatory regime, one must abandon the effective fluid descrip-

tion of dark energy and work directly with the fundamental perturbation variables of the theory. In practice, this means evolving:

- the metric perturbation Ψ , and
- the scalar-field perturbation $\delta\phi$,

using the linearised Einstein equations (Eqs. (22)–(24)) together with the perturbed Klein–Gordon equation (28).

This formulation remains fully regular even when $\dot{\phi} = 0$ and is therefore valid across both oscillatory and non-oscillatory regimes. Matter and radiation continue to be treated as standard perfect fluids, while the scalar field is handled as a fundamental degree of freedom rather than an effective fluid.

In the next subsection, we specify the initial conditions used to solve the perturbation equations numerically, paying particular attention to the treatment of super-Hubble modes and the matching to adiabatic initial conditions at early-time.

C. Initial conditions

The numerical integration of the linear perturbation equations requires the specification of initial conditions at an early epoch. We choose the initial time such that

$$\ln(a_i/a_0) = -15, \quad (41)$$

which lies deep in the radiation-dominated era. At this time the radiation component dominates the total energy density, so that

$$\rho_i \simeq \rho_{ri}, \quad w_{\text{eff},i} \simeq \frac{1}{3}, \quad (42)$$

and the contribution of matter and of the scalar field to the background evolution is negligible. All Fourier modes considered in this work satisfy

$$k \ll \mathcal{H}_i, \quad (43)$$

and therefore lie well outside the Hubble radius.

In this super-Hubble regime, the growing solution of the perturbed Einstein equations corresponds to a constant Newtonian potential [56]. We select this mode by imposing

$$\Psi'_i = 0. \quad (44)$$

Using the Einstein constraint equations, this condition relates the initial metric perturbation to the total density and velocity perturbations as

$$\Psi_i = -\frac{\delta_i}{2[1 + k^2/(3\mathcal{H}_i^2)]}, \quad \Psi_i = -\frac{3}{2}\mathcal{H}_i v_i (1 + w_{\text{eff},i}). \quad (45)$$

Although the initial conditions are imposed in the limit $k/\mathcal{H}_i \ll 1$, we retain the term proportional to $(k/\mathcal{H}_i)^2$

in Eq. (45). This ensures that Ψ'_i vanishes exactly at the initial time and prevents the appearance of small numerical transients at the start of the integration.

We assume adiabatic initial conditions for the fluid components. Adiabaticity implies that the density perturbations satisfy [59]

$$\frac{\delta_{ri}}{1 + w_r} = \frac{\delta_{mi}}{1 + w_m} = \frac{\delta_i}{1 + w_{\text{eff},i}}, \quad (46)$$

and that all components share a common velocity potential,

$$v_{ri} = v_{mi} = v_i, \quad (47)$$

with $w_r = 1/3$ and $w_m = 0$. Combining Eqs. (45)–(47), the initial density and velocity perturbations are completely fixed in terms of Ψ_i and $w_{\text{eff},i}$. At the initial time considered here, radiation domination implies $w_{\text{eff},i} \simeq 1/3$.

In contrast to the fluid components, the scalar field is treated as a fundamental degree of freedom rather than as an effective fluid. For numerical convenience, we choose

$$\delta\phi_i = 0, \quad \delta\phi'_i = 0. \quad (48)$$

These conditions do not enforce exact adiabaticity in the scalar-field sector at the initial time. However, this choice has no impact on the physical predictions of the model. At $a = a_i$ the scalar field is dynamically subdominant, $\Omega_\phi(a_i) \ll 1$, so its perturbations do not contribute appreciably to the Einstein constraints. Moreover, on super-Hubble scales during radiation domination, the coupled Einstein–Klein–Gordon system admits an attractive adiabatic growing mode. As a result, the evolution rapidly converges toward the adiabatic solution before horizon entry for the modes of interest, as we show in Appendix A.

For the numerical calculations we set $\Psi_i = 1$. Physical amplitudes are restored *a posteriori* by rescaling the solutions using the primordial perturbation amplitude inferred from cosmic microwave background observations. Concretely, the dimensionless numerical solutions are multiplied by the factor

$$\mathcal{A}(k) = \frac{2\pi}{3} \sqrt{2A_s} \left(\frac{k}{k_{\text{pivot}}} \right)^{\frac{n_s-1}{2}} k^{-3/2}, \quad (49)$$

which relates the initial Newtonian potential to the primordial curvature power spectrum generated during inflation. Throughout this work we adopt $\ln(10^{10}A_s) = 3.0448$, $n_s = 0.96605$, and $k_{\text{pivot}} = 0.05 \text{ Mpc}^{-1}$, motivated by the Planck 2018 results [17]. We note that, unlike the background parameter H_0 , which we choose to lie between the Planck and Type Ia supernova preferred values, the primordial parameters (A_s, n_s) are constrained by CMB anisotropies and are not informed by supernova data. It is therefore natural to adopt the Planck-preferred values when normalising the perturbation spectrum.

IV. NUMERICAL RESULTS

In this section we present the numerical solutions of the linear perturbation equations derived in the previous section. Our aim is to characterise the behaviour of scalar-field and matter perturbations in generalised axion-like quintessence models, with particular emphasis on the oscillatory regime and its impact on structure formation. We first analyse the evolution of the perturbations themselves and then examine the resulting signatures in cosmological observables.

A. Scalar-field and matter perturbations

We now analyse the numerical evolution of scalar-field and matter perturbations and their dependence on the underlying dark-energy dynamics. This joint discussion allows us to assess both the regularity of the perturbations in the oscillatory regime and the impact of the scalar field on the growth of cosmic structure.

Figure 3 shows the evolution of the scalar-field perturbations (left panel) and the matter density perturbations (right panel) for several Fourier modes, comparing a non-oscillatory model with an oscillatory one. In all cases, the perturbations remain finite and well behaved throughout the entire evolution. In particular, no divergences appear when the background scalar field crosses points where $\dot{\phi} = 0$. This confirms that the field-based formulation adopted in this work provides a fully regular description of linear perturbations, even in the presence of rapid oscillations.

The appearance of oscillations in $\delta\phi$ for the background-oscillatory solutions can be understood from the structure of the scalar-field perturbation equation (28), which takes the form of a damped, driven oscillator for each Fourier mode. The effective frequency is set by the combination $k^2 + a^2 V_{,\phi\phi}(\bar{\phi})$, while the perturbations are sourced by the metric and background evolution through terms proportional to $\bar{\phi}'$ and $V_{,\phi}(\bar{\phi})$. Once the background field oscillates around the minimum of the potential, both $\bar{\phi}'$ and $V_{,\phi}(\bar{\phi}) \simeq m_{\text{eff}}^2(\bar{\phi} - \phi_{\text{min}})$ inherit the same oscillatory time dependence, so that the source term becomes oscillatory and naturally excites an oscillatory response in $\delta\phi$, even though the perturbations remain perfectly regular throughout the evolution. In addition, near the minimum of the potential the curvature $V_{,\phi\phi}(\bar{\phi})$ is approximately constant and equal to m_{eff}^2 , so that the homogeneous part of the perturbation equation admits oscillatory solutions whenever this scale dominates over Hubble damping. This situation is realised in the oscillatory benchmark, whereas in the non-oscillatory case the scalar field remains effectively overdamped at late-time, suppressing any coherent oscillatory pattern in $\delta\phi$.

The amplitude of the scalar-field perturbations is larger in the non-oscillatory case. In this regime the scalar field remains in a tracking phase until relatively

late-time, with an equation of state that deviates appreciably from $w_\phi = -1$. During tracking, the scalar field develops comparatively larger fluctuations, leading to a higher late-time amplitude of $\delta\phi$. In contrast, in the oscillatory case the scalar field has a larger effective mass and exits the tracking regime earlier. Once the scalar-field energy density becomes relevant, its equation of state rapidly approaches $w_\phi \simeq -1$ and subsequently oscillates around this value. As a result, the scalar-field perturbations are suppressed and their amplitude remains small, approaching the Λ CDM limit, where dark energy does not cluster.

A complementary behaviour is observed in the matter sector. In the oscillatory case, the scalar field behaves effectively as a cosmological constant by late-time, and the evolution of matter perturbations is practically indistinguishable from that of Λ CDM. Any suppression of matter clustering is therefore negligible. In contrast, in the non-oscillatory case the prolonged tracking phase leads to a late-time suppression of matter perturbations. Since the scalar field contributes non-negligibly to the total energy density while maintaining an equation of state significantly different from -1 , the expansion history and the gravitational potentials driving structure formation are modified, resulting in a reduced growth rate and less efficient clustering. As we will show in the next subsection, this suppression translates directly into observable signatures and can be used to constrain the parameter space of the model [23].

B. Cosmological observables

We conclude our numerical analysis by examining the impact of the scalar-field dynamics on cosmological observables related to structure formation. In particular, we focus on the matter power spectrum and on the quantity $f\sigma_8$, both of which provide direct observational probes of the growth of matter perturbations. As we show below, these observables encode the same qualitative behaviour already identified at the level of linear perturbations.

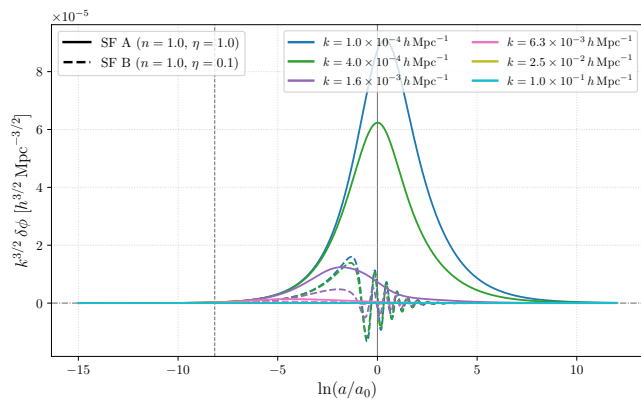
In the Newtonian gauge adopted throughout this work, the (dimensionless) matter power spectrum can be expressed as [57]

$$P(k, z) = |\delta_m(k, z) - 3\mathcal{H}(z) v_m(k, z)|^2, \quad (50)$$

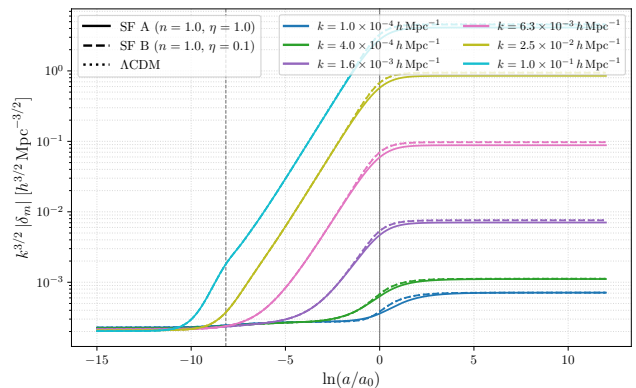
where δ_m and v_m denote the matter density contrast and velocity potential, respectively, and \mathcal{H} is the conformal Hubble rate. This quantity characterises the distribution of matter fluctuations as a function of scale.

Another widely used observable in large-scale structure analyses is $f\sigma_8$, which combines the growth rate of matter perturbations [60],

$$f(z) \equiv \frac{d \ln \delta_m}{d \ln a}, \quad (51)$$



(a) Evolution of the scalar-field perturbations $k^{3/2}\delta\phi$ as a function of $\ln(a/a_0)$ for several Fourier modes. The perturbations remain finite and well behaved throughout the evolution. The non-oscillatory model exhibits larger amplitudes, while in the oscillatory case the perturbations are suppressed as the scalar-field equation of state rapidly approaches and oscillates around $w_\phi = -1$.



(b) Evolution of the matter density perturbations $k^{3/2}|\delta_m|$ for the same set of Fourier modes. In the non-oscillatory case a late-time suppression of matter clustering is observed due to the prolonged tracking regime. In contrast, in the oscillatory case the evolution of matter perturbations is practically indistinguishable from that of ΛCDM .

Figure 3: Scalar-field and matter perturbations for generalised axion-like quintessence models. The left panel shows the evolution of the scalar-field perturbations, highlighting their regular behaviour across the oscillatory regime. The right panel shows the corresponding matter density perturbations, illustrating the suppression present in the non-oscillatory case and its absence in the oscillatory case, where the dynamics closely resemble ΛCDM .

with the rms amplitude of matter fluctuations on scales of $8 h^{-1} \text{ Mpc}$, denoted by σ_8 . Its redshift evolution is given by [61]

$$\sigma_8(z) = \sigma_8(0) \frac{\delta_m(z, k_{\sigma_8})}{\delta_m(0, k_{\sigma_8})}, \quad (52)$$

where $k_{\sigma_8} = 0.125 h \text{ Mpc}^{-1}$ corresponds to a comoving scale of $8 h^{-1} \text{ Mpc}$ and we take $\sigma_8(0) = 0.8120$ [17]. The product $f\sigma_8$ is particularly useful, as it is largely insensitive to galaxy bias and can be directly compared with observational data.

Figure 4 summarises our results. The left panel shows the matter power spectrum at $z = 0$ for the non-oscillatory and oscillatory benchmark models, compared with the ΛCDM prediction. The right panel displays the evolution of $f\sigma_8$ at low redshift, together with observational data.

In the non-oscillatory case, the matter power spectrum exhibits a clear suppression with respect to ΛCDM over a wide range of scales. This suppression is a direct consequence of the prolonged tracking regime discussed in the previous subsection. Since the scalar field departs significantly from $w_\phi = -1$ while contributing non-negligibly to the total energy density, the growth of matter perturbations is reduced, leading to less efficient clustering and a lower amplitude of the power spectrum at late-time. The same effect is reflected in the evolution of $f\sigma_8$, which is systematically suppressed at low redshift.

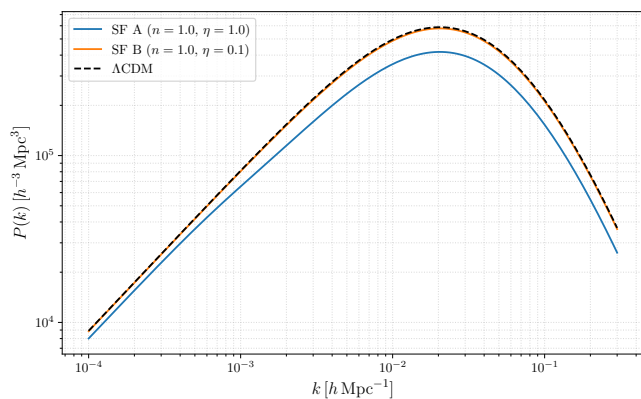
In contrast, in the oscillatory case the deviations from ΛCDM are significantly reduced. Owing to the larger effective mass of the scalar field, the tracking regime

ends earlier and the equation of state rapidly approaches $w_\phi \simeq -1$ once the scalar-field energy density becomes relevant. As a result, the late-time expansion history and the growth of structures closely resemble those of ΛCDM . This behaviour is clearly visible in both observables: the matter power spectrum closely follows the ΛCDM prediction, and the evolution of $f\sigma_8$ remains well within current observational bounds.

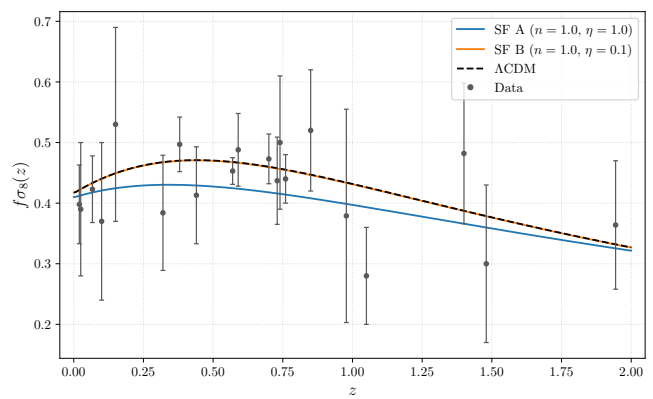
Overall, these results demonstrate that structure-formation observables provide a powerful discriminator between different scalar-field dynamics. While non-oscillatory models with extended tracking phases are subject to strong constraints due to their suppression of matter clustering, oscillatory models naturally evade these bounds by approaching a cosmological-constant-like behaviour at late-time, rendering them largely indistinguishable from ΛCDM .

V. CONCLUSIONS

We have investigated late-time cosmic acceleration driven by a generalised axion-like quintessence field in the regime in which the scalar field executes coherent oscillations around the finite, positive minimum of its potential. This oscillatory phase is a distinctive feature of the class of models considered here, and it has a direct impact on the formulation of linear cosmological perturbations. In particular, we have shown that the commonly used effective multi-fluid description of dark energy becomes ill defined once oscillations occur: although the background



(a) Matter power spectrum at $z = 0$ for the non-oscillatory and oscillatory benchmark models, compared with Λ CDM. A clear suppression is observed in the non-oscillatory case due to the prolonged tracking regime, while in the oscillatory case the spectrum closely follows the Λ CDM prediction.



(b) Evolution of $f\sigma_8$ as a function of redshift for the same benchmark models, compared with Λ CDM and observational data [62]. The non-oscillatory model exhibits a noticeable suppression at low redshift, while the oscillatory case remains close to the Λ CDM prediction.

Figure 4: Cosmological observables in generalised axion-like quintessence models. The left panel shows the matter power spectrum at $z = 0$, while the right panel displays the evolution of $f\sigma_8$ at low redshift. Both observables reflect the same qualitative behaviour found at the level of linear perturbations: significant suppression in the non-oscillatory case and near- Λ CDM behaviour in the oscillatory case.

quantities remain regular, fluid variables such as the adiabatic sound speed and combinations involving $1 + w_\phi$ develop turning-point divergences when the field reaches $w_\phi = -1$ at each oscillation.

To address this issue, we developed and implemented a field-based perturbation framework that evolves the fundamental variables $(\Psi, \delta\phi)$ together with standard matter and radiation perturbations in the Newtonian gauge. This formulation remains fully regular across the entire evolution, including at the turning points where $\dot{\phi} = 0$, because the Einstein equations are sourced only by the regular combinations $\delta\rho$, δp , and $(\bar{\rho} + \bar{p})v$. As a result, the metric perturbation Ψ and all physical perturbations remain smooth even when the mapping to fluid variables breaks down. This provides a consistent and robust route to study structure formation in oscillating quintessence models without relying on ill-defined effective fluid quantities.

Using numerical solutions, we characterised the behaviour of scalar-field and matter perturbations and connected them to late-time observables. We found that the amplitude and phenomenology depend strongly on whether the model is non-oscillatory or oscillatory by today, which is controlled by the comparison between the effective mass near the minimum and the Hubble scale. In non-oscillatory solutions, the scalar field can remain in a prolonged tracking phase with w_ϕ appreciably different from -1 , leading to a noticeable late-time suppression of matter clustering. This suppression propagates to structure-formation observables, yielding a reduced matter power spectrum amplitude and a systematically lower $f\sigma_8$ at low redshift relative to Λ CDM. In oscillatory solutions, instead, the field approaches a

cosmological-constant-like behaviour once it becomes dynamically relevant and subsequently oscillates around $w_\phi \simeq -1$, which suppresses scalar-field perturbations and makes the growth of matter perturbations and the associated observables closely track the Λ CDM predictions.

Overall, our results show that oscillatory generalised axion-like quintessence can naturally evade late-time growth constraints that are more restrictive for non-oscillatory tracking-like models, while still providing a dynamical origin for dark energy. Beyond this qualitative conclusion, the main outcome of this work is methodological: the field-based perturbation treatment derived here supplies a unified, well-defined framework to explore the full parameter space of these models, including regions in which fluid-based approaches fail.

Appendix A: Fluid-pathology diagnostics and regularity of the metric perturbation

The oscillatory regime discussed in the main text highlights a well-known limitation of the effective multi-fluid description of a canonical scalar field. In particular, during coherent oscillations around the minimum of the potential, the background equation of state w_ϕ periodically reaches -1 at the turning points of the motion, i.e. when $\dot{\phi}' = 0$. While the fundamental perturbation variables $(\delta\phi, \delta\phi')$ remain regular, several *fluid* quantities commonly used in the multi-fluid framework become ill-defined at those instants. This appendix provides a numerical diagnostic of this pathology and shows explicitly that it does *not* propagate to the metric perturbations, which remain perfectly regular.

Scalar-field perturbations in field variables. In the Newtonian gauge and in conformal time, the scalar-field energy-density, pressure, and momentum-density perturbations can be written directly in terms of $\delta\phi$ as

$$\delta\rho_\phi = \frac{1}{a^2} \left(\bar{\phi}' \delta\phi' - \bar{\phi}'^2 \Psi \right) + V_{,\phi}(\bar{\phi}) \delta\phi, \quad (\text{A1})$$

$$\delta p_\phi = \frac{1}{a^2} \left(\bar{\phi}' \delta\phi' - \bar{\phi}'^2 \Psi \right) - V_{,\phi}(\bar{\phi}) \delta\phi, \quad (\text{A2})$$

$$(\bar{\rho}_\phi + \bar{p}_\phi) v_\phi = -\frac{\bar{\phi}'}{a^2} \delta\phi, \quad (\text{A3})$$

where an overbar denotes a background quantity and $V_{,\phi} \equiv dV/d\phi$. The background density and pressure are

$$\bar{\rho}_\phi = \frac{\bar{\phi}'^2}{2a^2} + V(\bar{\phi}), \quad \bar{p}_\phi = \frac{\bar{\phi}'^2}{2a^2} - V(\bar{\phi}), \quad w_\phi \equiv \frac{\bar{p}_\phi}{\bar{\rho}_\phi}. \quad (\text{A4})$$

Therefore,

$$1 + w_\phi = \frac{\bar{\rho}_\phi + \bar{p}_\phi}{\bar{\rho}_\phi} = \frac{\bar{\phi}'^2}{a^2 \bar{\rho}_\phi}, \quad (\text{A5})$$

so that $1 + w_\phi = 0$ precisely when $\bar{\phi}' = 0$, i.e. when w_ϕ reaches -1 .

A diagnostic of the multi-fluid pathology. A commonly used ‘‘adiabatic-like’’ combination in the fluid treatment is $\delta\phi/(1 + w_\phi)$, where $\delta\phi \equiv \delta\rho_\phi/\bar{\rho}_\phi$. Using (A1)–(A5), we can write

$$\frac{\delta\phi}{1 + w_\phi} = \frac{\delta\rho_\phi/\bar{\rho}_\phi}{\bar{\phi}'^2/(a^2 \bar{\rho}_\phi)} = \frac{\bar{\phi}' \delta\phi' - \bar{\phi}'^2 \Psi + a^2 V_{,\phi} \delta\phi}{\bar{\phi}'^2}. \quad (\text{A6})$$

Even though $\delta\rho_\phi$, δp_ϕ , and $(\bar{\rho}_\phi + \bar{p}_\phi)v_\phi$ remain finite, the ratio (A6) diverges whenever $\bar{\phi}' = 0$ (equivalently when w_ϕ reaches -1). The same turning-point pathology underlies the divergence of other fluid variables, such as the scalar-field velocity potential

$$v_\phi = -\frac{\delta\phi}{\bar{\phi}'}, \quad (\text{A7})$$

and the adiabatic sound speed $c_{a,\phi}^2 \equiv \bar{p}'_\phi/\bar{\rho}'_\phi$. Importantly, these divergences are *kinematical* and do not signal any physical instability: they simply reflect the breakdown of the mapping from field variables to a fluid description at the turning points of the background evolution.

Metric equations remain regular. In the Einstein equations, the metric perturbation is sourced by the *total* density perturbation, momentum density, and pressure perturbation. In the notation used in the main text (total quantities without subindices), the sources that enter the linearised Einstein equations are

$$\delta\rho = \delta\rho_m + \delta\rho_r + \delta\rho_\phi, \quad (\text{A8})$$

$$\delta p = \delta p_r + \delta p_\phi, \quad (\text{A9})$$

$$(\bar{\rho} + \bar{p}) v = \sum_A (\bar{\rho}_A + \bar{p}_A) v_A. \quad (\text{A10})$$

For matter and radiation, all contributions are manifestly regular. For the scalar field, $\delta\rho_\phi$, δp_ϕ , and $(\bar{\rho}_\phi + \bar{p}_\phi)v_\phi$ are given by Eqs. (A1)–(A3) and remain finite throughout the oscillatory regime. Hence, even though fluid variables such as $\delta\phi/(1 + w_\phi)$, v_ϕ , and $c_{a,\phi}^2$ diverge at turning points, the combinations that actually source the metric do not, and the gravitational potential Ψ remains well behaved.

The behaviour discussed above is illustrated in Fig. 5. The left panel shows the fluid-pathology diagnostic $\delta\phi/(1 + w_\phi)$ for several Fourier modes, including both benchmark scalar-field models (non-oscillatory and oscillatory), and the Λ CDM case for comparison. Divergent spikes appear *only* in the oscillatory benchmark and occur at the same values of $\ln(a/a_0)$ for all modes, confirming that they are driven by background turning points at which w_ϕ reaches -1 , rather than by any scale-dependent instability. All the divergent peaks coincide with the minima of the oscillations in the scalar-field equation of state shown in Fig. 2b.

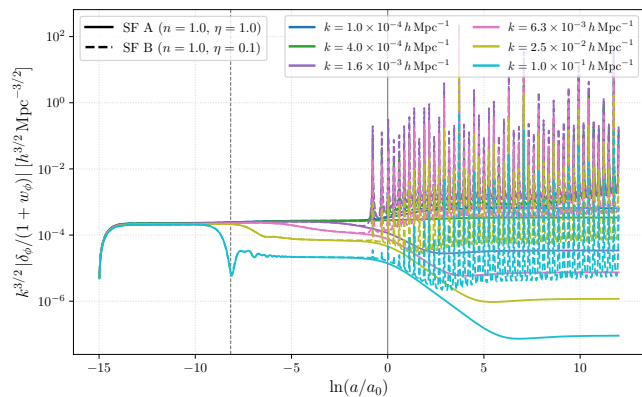
Although the majority of these turning points occur in the future for the benchmark oscillatory model shown here, some of them already take place close to the present epoch, making their treatment relevant for late-time cosmology. Moreover, models with larger effective masses—e.g. obtained by considering smaller values of η —exhibit more frequent oscillations, with multiple turning points occurring well before today. In all such cases, the standard fluid description becomes ill defined, independently of whether the turning points lie in the past or future. This motivates the use of the field-based perturbation framework developed in this work, which provides a consistent description across the full parameter space, including models with heavier fields and earlier oscillatory behaviour.

Finally, although the scalar-field perturbations are initialised with $\delta\phi_i = \delta\phi'_i = 0$, which does not strictly satisfy adiabatic initial conditions, the evolution rapidly converges to the adiabatic attractor on super-Hubble scales, as is clearly visible in the early-time behaviour of the fluid diagnostic.

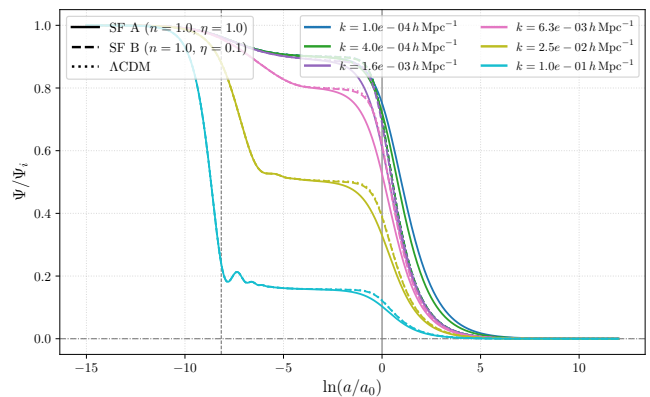
The right panel shows the evolution of the metric potential Ψ/Ψ_i for the same set of modes and models. Despite the fluid-pathology spikes present in the oscillatory scalar-field benchmark, Ψ remains finite and smooth at all times. This confirms that the apparent divergences arising in the multi-fluid description do not propagate to the metric sector, since the Einstein equations are sourced only by the regular combinations $\delta\rho$, $(\bar{\rho} + \bar{p})v$, and δp .

ACKNOWLEDGEMENTS

The authors are grateful to Hsu-Wen Chiang for his helpful comments on this work. M. B.-L. is supported by the Basque Foundation of Science Ikerbasque. C. G. B. acknowledges financial support from the FPI fellow-



(a) Evolution of the “adiabatic-like” fluid diagnostic $k^{3/2} |\delta_\phi / (1 + w_\phi)| |h^{3/2} \text{Mpc}^{-3/2}|$ for the benchmark models. The divergent spikes occur only in the oscillatory benchmark and appear whenever the background equation of state reaches $w_\phi = -1$ (equivalently $\dot{\phi}' = 0$). The locations of the peaks are independent of the mode k , as expected since the turning points are fixed by the background dynamics. In the non-oscillatory benchmark no such spikes arise.



(b) Evolution of the metric potential Ψ/Ψ_i for the same set of modes and models (non-oscillatory and oscillatory scalar-field benchmarks, and ΛCDM). No pathology is observed: Ψ remains finite and smooth throughout the oscillatory regime because the Einstein equations are sourced by the regular combinations $\delta\rho$, $(\bar{\rho} + \bar{p})v$, and δp (cf. (A8)), rather than by ill-defined fluid variables such as $\delta_\phi / (1 + w_\phi)$, v_ϕ , or $c_{a,\phi}^2$.

Figure 5: Diagnostic of the breakdown of the multi-fluid description in the oscillatory regime and regularity of the metric perturbation. The left panel shows that the fluid diagnostic $\delta_\phi / (1 + w_\phi)$ develops turning-point divergences only for the oscillatory benchmark. The right panel shows that this behaviour does not propagate to the metric: the gravitational potential remains well defined and well behaved, and closely follows the corresponding smooth evolution in the non-oscillatory benchmark and in ΛCDM .

ship PRE2021-100340 of the Spanish Ministry of Science, Innovation and Universities. Our work is supported by the Spanish Grant PID2023-149016NB-I00

(MINECO/AEI/FEDER, UE). This work is also supported by the Basque government Grant No. IT1628-22 (Spain).

-
- [1] B. Ratra and P. J. E. Peebles, Cosmological Consequences of a Rolling Homogeneous Scalar Field, *Phys. Rev. D* **37**, 3406 (1988).
 - [2] C. Wetterich, Cosmology and the Fate of Dilatation Symmetry, *Nucl. Phys. B* **302**, 668 (1988), arXiv:1711.03844 [hep-th].
 - [3] R. R. Caldwell, R. Dave, and P. J. Steinhardt, Cosmological imprint of an energy component with general equation of state, *Phys. Rev. Lett.* **80**, 1582 (1998), arXiv:astro-ph/9708069.
 - [4] P. G. Ferreira and M. Joyce, Cosmology with a primordial scaling field, *Phys. Rev. D* **58**, 023503 (1998), arXiv:astro-ph/9711102.
 - [5] I. Zlatev, L.-M. Wang, and P. J. Steinhardt, Quintessence, cosmic coincidence, and the cosmological constant, *Phys. Rev. Lett.* **82**, 896 (1999), arXiv:astro-ph/9807002.
 - [6] A. R. Liddle and R. J. Scherrer, A Classification of scalar field potentials with cosmological scaling solutions, *Phys. Rev. D* **59**, 023509 (1999), arXiv:astro-ph/9809272.
 - [7] P. J. Steinhardt, L.-M. Wang, and I. Zlatev, Cosmological tracking solutions, *Phys. Rev. D* **59**, 123504 (1999), arXiv:astro-ph/9812313.
 - [8] S. Tsujikawa, Quintessence: A Review, *Class. Quant. Grav.* **30**, 214003 (2013), arXiv:1304.1961 [gr-qc].
 - [9] R. Bean, S. H. Hansen, and A. Melchiorri, Early-universe constraints on dark energy, *Phys. Rev. D* **64**, 103508 (2001).
 - [10] L. Amendola and S. Tsujikawa, *Dark Energy: Theory and Observations* (Cambridge University Press, 2015).
 - [11] R. R. Caldwell and E. V. Linder, The Limits of quintessence, *Phys. Rev. Lett.* **95**, 141301 (2005), arXiv:astro-ph/0505494.
 - [12] T. G. Clemons and A. R. Liddle, Observational constraints on thawing quintessence models, *Mon. Not. Roy. Astron. Soc.* **395**, 1585 (2009), arXiv:0811.4676 [astro-ph].
 - [13] T. Chiba, A. De Felice, and S. Tsujikawa, Observational constraints on quintessence: thawing, tracker, and scaling models, *Phys. Rev. D* **87**, 083505 (2013), arXiv:1210.3859 [astro-ph.CO].
 - [14] A. G. Riess *et al.* (Supernova Search Team), Observational evidence from supernovae for an accelerating universe and a cosmological constant, *Astron. J.* **116**, 1009 (1998), arXiv:astro-ph/9805201.
 - [15] S. Perlmutter *et al.* (Supernova Cosmology Project), Measurements of Ω and Λ from 42 High Redshift Su-

- pernovae, *Astrophys. J.* **517**, 565 (1999), [arXiv:astro-ph/9812133](#).
- [16] D. Brout *et al.*, The Pantheon+ Analysis: Cosmological Constraints, *Astrophys. J.* **938**, 110 (2022), [arXiv:2202.04077 \[astro-ph.CO\]](#).
- [17] N. Aghanim *et al.* (Planck), Planck 2018 results. VI. Cosmological parameters, *Astron. Astrophys.* **641**, A6 (2020), [Erratum: *Astron. Astrophys.* 652, C4 (2021)], [arXiv:1807.06209 \[astro-ph.CO\]](#).
- [18] D. J. Eisenstein *et al.* (SDSS), Detection of the Baryon Acoustic Peak in the Large-Scale Correlation Function of SDSS Luminous Red Galaxies, *Astrophys. J.* **633**, 560 (2005), [arXiv:astro-ph/0501171](#).
- [19] S. Cole *et al.* (2dFGRS), The 2dF Galaxy Redshift Survey: Power-spectrum analysis of the final dataset and cosmological implications, *Mon. Not. Roy. Astron. Soc.* **362**, 505 (2005), [arXiv:astro-ph/0501174](#).
- [20] W. J. Percival, B. A. Reid, D. J. Eisenstein, N. A. Bahcall, T. Budavari, J. A. Frieman, M. Fukugita, J. E. Gunn, Ž. Ivezić, G. R. Knapp, *et al.*, Baryon acoustic oscillations in the sloan digital sky survey data release 7 galaxy sample, *Monthly Notices of the Royal Astronomical Society* **401**, 2148 (2010).
- [21] M. Tegmark *et al.* (SDSS), The 3-D power spectrum of galaxies from the SDSS, *Astrophys. J.* **606**, 702 (2004), [arXiv:astro-ph/0310725](#).
- [22] B. A. Reid *et al.*, Cosmological Constraints from the Clustering of the Sloan Digital Sky Survey DR7 Luminous Red Galaxies, *Mon. Not. Roy. Astron. Soc.* **404**, 60 (2010), [arXiv:0907.1659 \[astro-ph.CO\]](#).
- [23] H.-W. Chiang, C. G. Boiza, and M. Bouhmadi-López, Observational constraints on generalised axion-like potentials for the late Universe, *JCAP* **08**, 064, [arXiv:2503.04898 \[astro-ph.CO\]](#).
- [24] M. Bouhmadi-López, H.-W. Chiang, and C. G. Boiza, Generalised axion-like dark energy: From theory to observations, *Phys. Dark Univ.* **49**, 101968 (2025).
- [25] M. W. Hossain and A. Maqsood, Cosmological implications of tracker scalar fields: Testing the evidence for dynamical dark energy with recent data, *Phys. Rev. D* **112**, 083504 (2025), [arXiv:2502.19274 \[astro-ph.CO\]](#).
- [26] A. G. Adame *et al.* (DESI), DESI 2024 III: baryon acoustic oscillations from galaxies and quasars, *JCAP* **04**, 012, [arXiv:2404.03000 \[astro-ph.CO\]](#).
- [27] A. G. Adame *et al.* (DESI), DESI 2024 IV: Baryon Acoustic Oscillations from the Lyman alpha forest, *JCAP* **01**, 124, [arXiv:2404.03001 \[astro-ph.CO\]](#).
- [28] A. G. Adame *et al.* (DESI), DESI 2024 VI: cosmological constraints from the measurements of baryon acoustic oscillations, *JCAP* **02**, 021, [arXiv:2404.03002 \[astro-ph.CO\]](#).
- [29] M. Abdul Karim *et al.* (DESI), DESI DR2 results. II. Measurements of baryon acoustic oscillations and cosmological constraints, *Phys. Rev. D* **112**, 083515 (2025), [arXiv:2503.14738 \[astro-ph.CO\]](#).
- [30] J. A. Frieman, C. T. Hill, A. Stebbins, and I. Waga, Cosmology with ultralight pseudo Nambu-Goldstone bosons, *Phys. Rev. Lett.* **75**, 2077 (1995), [arXiv:astro-ph/9505060](#).
- [31] M. Kamionkowski, J. Pradler, and D. G. E. Walker, Dark energy from the string axiverse, *Phys. Rev. Lett.* **113**, 251302 (2014), [arXiv:1409.0549 \[hep-ph\]](#).
- [32] R. Emami, D. Grin, J. Pradler, A. Raccanelli, and M. Kamionkowski, Cosmological tests of an axiverse-inspired quintessence field, *Phys. Rev. D* **93**, 123005 (2016), [arXiv:1603.04851 \[astro-ph.CO\]](#).
- [33] D. J. E. Marsh, Axion Cosmology, *Phys. Rept.* **643**, 1 (2016), [arXiv:1510.07633 \[astro-ph.CO\]](#).
- [34] M. W. Hossain and A. Maqsood, Comparison between axionlike and power law potentials in a cosmological background, *Phys. Rev. D* **109**, 103512 (2024), [arXiv:2311.17825 \[astro-ph.CO\]](#).
- [35] C. G. Boiza and M. Bouhmadi-López, Speeding up the Universe with a generalised axion-like potential, *Eur. Phys. J. C* **85**, 777 (2025), [arXiv:2409.18184 \[astro-ph.CO\]](#).
- [36] C. G. Boiza and M. Bouhmadi-López, Cosmological perturbations in a generalised axion-like dark energy model, *Phys. Dark Univ.* **48**, 101845 (2025), [arXiv:2410.22467 \[astro-ph.CO\]](#).
- [37] V. Poulin, T. L. Smith, T. Karwal, and M. Kamionkowski, Early Dark Energy Can Resolve The Hubble Tension, *Phys. Rev. Lett.* **122**, 221301 (2019), [arXiv:1811.04083 \[astro-ph.CO\]](#).
- [38] M. Kamionkowski and A. G. Riess, The Hubble Tension and Early Dark Energy, *Ann. Rev. Nucl. Part. Sci.* **73**, 153 (2023), [arXiv:2211.04492 \[astro-ph.CO\]](#).
- [39] A. Smith, M. Mylova, C. van de Bruck, C. P. Burgess, and E. Di Valentino, The Serendipitous Axiodilaton: A Self-Consistent Recombination-Era Solution to the Hubble Tension (2025), [arXiv:2512.13544 \[astro-ph.CO\]](#).
- [40] K. Freese, J. A. Frieman, and A. V. Olinto, Natural Inflation with Pseudo - Nambu-Goldstone Bosons, *Phys. Rev. Lett.* **65**, 3233 (1990).
- [41] M. Y. Khlopov, S. G. Rubin, and A. S. Sakharov, Primordial structure of massive black hole clusters, *Astropart. Phys.* **23**, 265 (2005), [arXiv:astro-ph/0401532](#).
- [42] M. Y. Khlopov, A. S. Sakharov, and D. D. Sokoloff, The nonlinear modulation of the density distribution in standard axionic CDM and its cosmological impact, *Nucl. Phys. B Proc. Suppl.* **72**, 105 (1999).
- [43] L. Hui, J. P. Ostriker, S. Tremaine, and E. Witten, Ultralight scalars as cosmological dark matter, *Phys. Rev. D* **95**, 043541 (2017), [arXiv:1610.08297 \[astro-ph.CO\]](#).
- [44] H.-Y. Schive, T. Chiueh, and T. Broadhurst, Cosmic Structure as the Quantum Interference of a Coherent Dark Wave, *Nature Phys.* **10**, 496 (2014), [arXiv:1406.6586 \[astro-ph.GA\]](#).
- [45] H.-Y. Schive, M.-H. Liao, T.-P. Woo, S.-K. Wong, T. Chiueh, T. Broadhurst, and W. Y. P. Hwang, Understanding the Core-Halo Relation of Quantum Wave Dark Matter from 3D Simulations, *Phys. Rev. Lett.* **113**, 261302 (2014), [arXiv:1407.7762 \[astro-ph.GA\]](#).
- [46] P. Mocz *et al.*, Galaxy formation with BECDM – II. Cosmic filaments and first galaxies, *Mon. Not. Roy. Astron. Soc.* **494**, 2027 (2020), [arXiv:1911.05746 \[astro-ph.CO\]](#).
- [47] D. J. Eisenstein and W. Hu, Baryonic features in the matter transfer function, *Astrophys. J.* **496**, 605 (1998), [arXiv:astro-ph/9709112](#).
- [48] D. J. Fixsen, The Temperature of the Cosmic Microwave Background, *Astrophys. J.* **707**, 916 (2009), [arXiv:0911.1955 \[astro-ph.CO\]](#).
- [49] V. F. Mukhanov, H. A. Feldman, and R. H. Brandenberger, Theory of cosmological perturbations. Part 1. Classical perturbations. Part 2. Quantum theory of perturbations. Part 3. Extensions, *Phys. Rept.* **215**, 203 (1992).

- [50] C.-P. Ma and E. Bertschinger, Cosmological perturbation theory in the synchronous and conformal Newtonian gauges, *Astrophys. J.* **455**, 7 (1995), [arXiv:astro-ph/9506072](#).
- [51] R. H. Brandenberger, Lectures on the theory of cosmological perturbations, *Lect. Notes Phys.* **646**, 127 (2004), [arXiv:hep-th/0306071](#).
- [52] K. A. Malik and D. Wands, Cosmological perturbations, *Phys. Rept.* **475**, 1 (2009), [arXiv:0809.4944 \[astro-ph\]](#).
- [53] M. Malquarti and A. R. Liddle, Evolution of large scale perturbations in quintessence models, *Phys. Rev. D* **66**, 123506 (2002), [arXiv:astro-ph/0208562](#).
- [54] B. A. Bassett, S. Tsujikawa, and D. Wands, Inflation dynamics and reheating, *Rev. Mod. Phys.* **78**, 537 (2006), [arXiv:astro-ph/0507632](#).
- [55] A. Wang, D. Wands, and R. Maartens, Scalar field perturbations in Horava-Lifshitz cosmology, *JCAP* **03**, 013, [arXiv:0909.5167 \[hep-th\]](#).
- [56] D. Baumann, *Cosmology: Part III Mathematical Tripos* (University of Cambridge, 2015).
- [57] I. Albarran, M. Bouhmadi-López, and J. Morais, Cosmological perturbations in an effective and genuinely phantom dark energy Universe, *Phys. Dark Univ.* **16**, 94 (2017), [arXiv:1611.00392 \[astro-ph.CO\]](#).
- [58] J. M. Bardeen, Gauge Invariant Cosmological Perturbations, *Phys. Rev. D* **22**, 1882 (1980).
- [59] G. Ballesteros and J. Lesgourgues, Dark energy with non-adiabatic sound speed: initial conditions and detectability, *JCAP* **10**, 014, [arXiv:1004.5509 \[astro-ph.CO\]](#).
- [60] A. Balcerzak and T. Denkiewicz, Density perturbations in a finite scale factor singularity universe, *Phys. Rev. D* **86**, 023522 (2012), [arXiv:1202.3280 \[astro-ph.CO\]](#).
- [61] Y. Wang *et al.*, Designing a space-based galaxy redshift survey to probe dark energy, *Mon. Not. Roy. Astron. Soc.* **409**, 737 (2010), [arXiv:1006.3517 \[astro-ph.CO\]](#).
- [62] F. Avila, A. Bernui, A. Bonilla, and R. C. Nunes, Inferring $S_8(z)$ and $\gamma(z)$ with cosmic growth rate measurements using machine learning, *Eur. Phys. J. C* **82**, 594 (2022), [arXiv:2201.07829 \[astro-ph.CO\]](#).